Nonlinear Transition to a Global Mode for Traveling-Wave Instability in a Finite box

Nicolas Garnier[1] and Arnaud Chiffaudel[1,2,*]

[1]*Service de Physique de l'État Condensé, CEA Saclay, 91191 Gif-sur-Yvette Cedex, France*

[2]*Département SPM, Section 5, Centre National de la Recherche Scientifique, 3, rue Michel Ange, 75016 Paris, France*

(Received 2 March 2000)

Using hydrothermal waves in a long narrow channel as an ideal supercritical nonlinear wave system, we study the critical behavior at onset for a finite cell with poorly reflecting boundaries. We observe a spatially nonuniform global eigenmode localized near the end of the cell and associated with a wave front invading the cell. The onset of this mode—corresponding to the absolute instability transition—is shifted above the value corresponding to convective instability, measured in an annular channel with periodic boundary conditions. Experimental critical exponents are discussed in the framework of existing theoretical descriptions and quantitative comparison with the complex Ginzburg-Landau model is attempted.

DOI: 10.1103/PhysRevLett.86.75 PACS numbers: 47.35.+i, 47.20.Dr, 47.27.Te, 47.54.+r

Since their first observations in large boxes, for example, in convecting binary fluids [1] or shear flows [2], nonlinear traveling waves have exhibited a fascinating variety of behaviors and patterns. We believe that in such systems the main source of richness near onset is the convective/absolute transition [3,4] for nonzero group velocity waves. Most 1D physical systems produce right- and left-propagating nonlinear waves [5]. Nonlinear competition and reflections at the boundaries lead to a central-source pattern [6–9] due to counterpropagating exponentially growing waves as the first global mode at onset. The global mode may also be produced by the convective/absolute transition. So far, this phenomenon was described for single waves [3,10,11], i.e., with broken left-right symmetry. Among systems, thermocapillary flows and, in particular, hydrothermal waves [12–15] may appear as the simplest models, owing to their supercritical bifurcation. This Letter is devoted to the case where two competing waves interact in a low-reflection boundaries cell. The first global mode, instead of being constructed by successive reflections in the convective regime, results thus from the absolute instability regime, high above the convective onset. In this region, we report the presence of sharp eigenmodes, precisely localized near the downstream boundary. These wall modes are similar to the solutions of perturbation analysis [3,10]. Furthermore, a nearly uniform nonlinearly saturated wave invades the cell at higher constraint by front propagation. This study addresses the delicate question of linear or nonlinear selection of global modes [16].

Experimental setup.—A narrow rectangular convection channel (Fig. 1) with a glass bottom and vertical copper walls [12] is filled with a thin layer, $h = (1.7 \pm 0.1)$ mm, of silicon oil of viscosity $\nu = 0.65$ cS (1 cS = 10^{-2} cm^2/s) and Prandtl number $P = 10$. The fluid surface is free. The channel is 10 mm wide and 250 mm long. Plexiglas blocks are inserted in the channel to reduce the length to $L = 180$ mm, i.e., aspect ratio $\Gamma = L/h \simeq 100$. The copper walls are thermoregulated by fluid circulations. Thermocouples allow accurate measurements of the temperature difference ΔT across the channel, typically established with a ± 15 mK stability. Convective patterns are observed through the glass bottom by shadowgraphy. Images are digitized and processed numerically as spatiotemporal diagrams of 512 data points extracted from the central line and plotted along time.

Basic flow and wave model.—The convective flow created by a horizontal thermal gradient has been previously described [12,14]. We use the same device as Daviaud and Vince except that we reduced the length in order to view the whole cell through a 200 mm lens. Data were also collected in a curved annular channel of 503 mm perimeter, i.e., with periodic boundary conditions, of identical 10 mm width, at the same $h = 1.7$ mm fluid height [14,17]. Because the curvature is negligible, both wave pattern reports can be directly connected. So let us summarize the results for annular geometry.

The first bifurcation of the basic thermocapillary flow towards hydrothermal waves occurs at $\Delta T_0 = (3.1 \pm 0.1)$ K [17]. The bifurcated pattern for hydrothermal waves is a uniform-amplitude traveling wave of critical wave number $k_0 = (0.684 \pm 0.003)$ mm^{-1} and critical frequency $f_0 = 0.237$ Hz [17]. The wave $\theta(x,t)$ is modeled by two slowly varying amplitudes A and B obeying two complex Ginzburg-Landau (CGL) equations:

$$\theta(x,t) = A(X,T)\exp i(\omega_0 t - k_0 x) + B(X,T)\exp i(\omega_0 t + k_0 x) + \text{c.c.} + \cdots,$$

$$\tau_0(A_T + sA_X) = \epsilon(1 + ic_0)A + \xi_0^2(1 + ic_1)A_{XX} - (1 + ic_2)|A|^2 A - (\lambda + i\mu)|B|^2 A,$$

$$\tau_0(B_T - sB_X) = \epsilon(1 + ic_0)B + \xi_0^2(1 + ic_1)B_{XX} - (1 + ic_2)|B|^2 B - (\lambda + i\mu)|A|^2 B,$$

where $\epsilon = \Delta T/\Delta T_0 - 1$. The group velocity $s = (0.895 \pm 0.01)$ mm^{-1} and the correlation length $\xi_0 = (5.1 \pm 0.3)$ mm have been measured in the annulus [17]. Perturbations are verified to travel at the velocity s in the rectangular box as well. Let us note that nondimensional

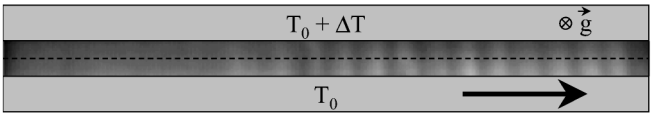

FIG. 1. Schematics of the channel with photograph of traveling hydrothermal waves and acquisition line (- - -).

lengths $L^* = L/\xi_0$ are 35 and 98 for the rectangular and the annular channels, respectively. We have shown $5s \lesssim \tau_0 \lesssim 15s$ and obtained some relations between c_0, c_1, and c_2. The coupling coefficient λ must be bigger than one because traveling waves are selected against standing waves [18]. From the practical point of view, we measure amplitude profiles $|A(X)|$ and $|B(X)|$, local wave numbers, and frequency. For this, we perform a temporal Hilbert transform [6,14] on the spatiotemporal data and then separate the right and left Fourier components without spatial filtering to keep the smallest scales of the envelopes.

Results in finite cell.—Typical amplitude profiles for A and B are shown in Fig. 2 for various temperature differences. For $\Delta T < \Delta T_a = 3.65$ K ($\epsilon < \epsilon_a = 0.177$), the profiles are flat $A = B = 0$. Just above onset, for $\Delta T = 3.66$ K, we observe a symmetric wave pattern. The

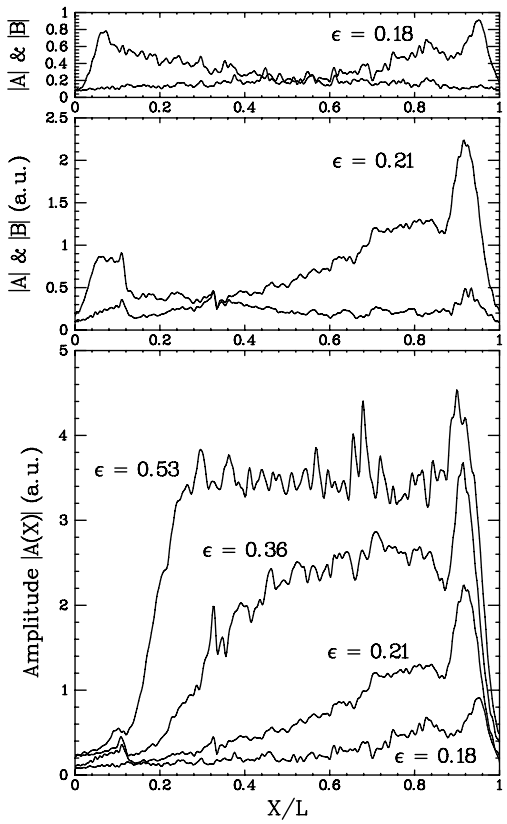

FIG. 2. Amplitude profiles of the traveling waves at different ϵ. Top figures present right (A) and left (B) amplitude profiles for $\epsilon = 0.18$ ($\Delta T = 3.66$ K) and $\epsilon = 0.21$ ($\Delta T = 3.75$ K). The bottom figure presents the dominant wave for growing ϵ up to 0.53 ($\Delta T = 4.75$ K). All dominant waves are represented as right-traveling waves. Following the wave, we encounter three domains: an exponential growth or front, a saturated plateau (for larger ϵ), and a sharp wall mode.

waves compete up to $\epsilon \simeq 0.25$, above which the smallest wave becomes negligible with respect to the dominant wave. The wave envelope of the latter may be separated in three domains: just after the wall $X = 0$, where both amplitudes are nearly zero, a front with exponential growing amplitude, then a plateau, and, finally, just before the end wall $X = L$, a sharp wall mode where the maximum amplitude is reached. The frequency and wave number are uniform along the cell except in the boundary layer and match the annulus critical values at onset (Fig. 3). Note that, for $\epsilon \gtrsim 0.3$, we observe quasiperiodic states corresponding to a beating of minor and major waves [6,8,9].

In the following we choose, for clarity, to present the major wave as A (right-traveling) and the minor wave as B (left-traveling), whereas the symmetric situation has been observed with equal probability. The plateau is vanishing in the threshold vicinity and so cannot be used to trace back the critical behavior. For a quantitative description of the bifurcation let us thus measure properties of the wall mode and the front regions.

Let us first look for the order parameter of the transition. The amplitude being nonuniform, two quantities are easily extracted: the mean and the maximum value of the amplitude profile. The average amplitude $\langle |A(X)| \rangle_{[0,L]}$ (not represented) evolves linearly with respect to ϵ (after a small finite step at ϵ_a). On the other hand, the maximum $A_{\max}$ which occurs near the downstream boundary, at the top of the wall mode, behaves like $(\epsilon - \epsilon_a)^{1/2}$ (Fig. 4a). We believe it to be the order parameter of this supercritical bifurcation. The ratio of the two amplitudes A and B, plotted in the inset, behaves like $\exp(-\alpha \frac{\epsilon - \epsilon_a}{\epsilon_a})$ with $\alpha = 3.0$ and denotes a strong competition between the two waves.

In order to modelize the spatial structure of the waves and the eigenmode near threshold, we measured the spatial evolution of the envelope $|A(X)|$. The front observed just at the wave source can be described by an exponential envelope $e^{\xi_F^{-1} X}$ with ξ_F^{-1} growth rate. The characteristic length ξ_F (Fig. 4b) appears thus, at first sight, to diverge at ϵ_a with critical exponent -1. At the other extremity, in the wave sink, the amplitude decreases and can be modelized by $e^{-\xi_B^{-1} X}$ where $\xi_B^{-1} = (39 \pm 4) L^{-1}$. Between the

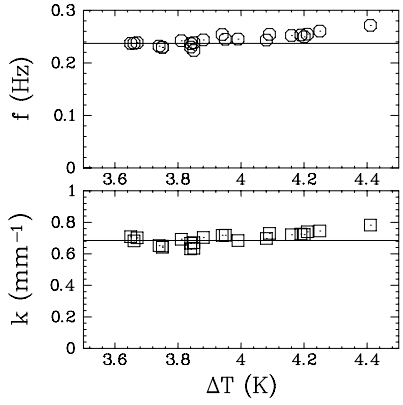

FIG. 3. Frequency and wave number vs ΔT. Horizontal lines show the critical values from annular cell data.

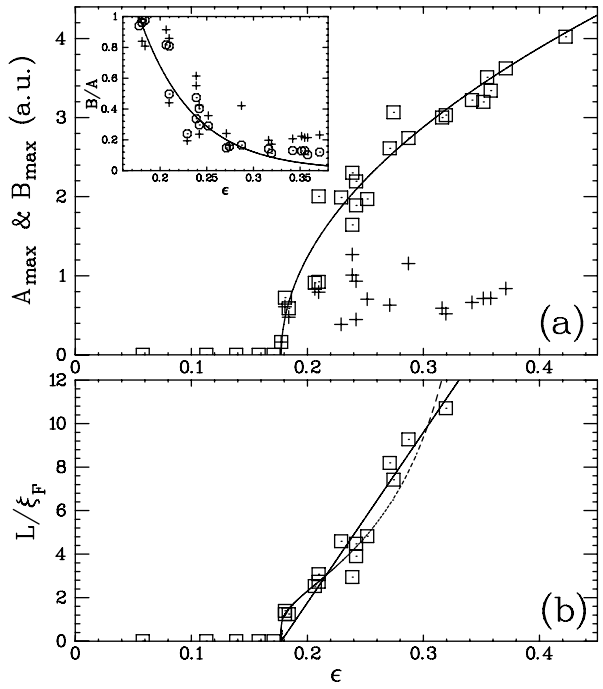

FIG. 4. (a) Modulus of the wall mode's amplitude or maximum amplitude vs ϵ. Dominant wave A (□) fitted by $(\epsilon - \epsilon_a)^{1/2}$ (solid line) and minor wave B (+). The inset presents the amplitude ratio B/A for mean amplitude over the cell (○) and maximum amplitudes (+). The solid line is an exponential fit. (b) Spatial growth rate ξ_F^{-1} of the envelope of the waves in the front region vs ϵ. Solid and dashed lines are linear—$\xi_F^{-1} \propto (\epsilon - \epsilon_a)$—and logarithmic fits, respectively (see text and Fig. 5).

plateau and the maximum, a small region in X as well as in ϵ, corresponding to the growing part of the wall mode, may also be fitted exponentially by $e^{\xi_{\mathrm{WM}}^{-1} X}$ where $\xi_{\mathrm{WM}}^{-1} = (15 \pm 1.5) L^{-1}$. These last two values do not significantly vary with ϵ.

Interpretation.—Three points need to be discussed and quantitatively compared to theoretical knowledge: (i) the onset shift between the annular cell and rectangular cell experiments, (ii) the shape of the wall mode, and (iii) the critical behavior of the front.

The shift of the onset is very large: 0.18 in ϵ or 0.55 K. Usual finite size effects are known to be of order $(\pi/L^*)^2$, i.e., 0.001 and 0.01 in ϵ for the $L^* = 98$ annulus and the $L^* = 35$ rectangular channel, respectively. This law has been verified with a good accuracy [19], in a variable rectangular cell. Another difference between the two cells is the curvature. This can be quantified by the stability analysis of the thermocapillary problem [15]: the annulus curvature increases the onset by 0.03 in ϵ. At this level, if the onset is observed for $\epsilon_c = 0$ in the annulus it is expected around -0.03 in the rectangle. None of these effects explains the 0.18 shift.

In the periodic channel, once the convective onset is crossed, a traveling wave (TW) self-organizes after successive rounds in the cell: the basic uniform TW is a global mode. So the convective onset is also the absolute onset

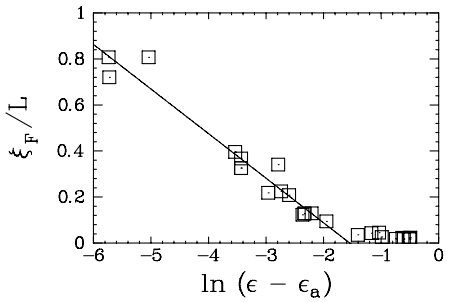

FIG. 5. Spatial growth length ξ_F of the envelope of the waves in the front region vs $\ln(\epsilon - \epsilon_a)$.

[3]. This corresponds mathematically to the static problem in a frame moving at group velocity s. In the nonperiodic channel, however, s is finite and the problem has to be solved in the laboratory frame. The first global mode, or self-excited wave, is observed above $\epsilon_a = 0.18$. Below ϵ_a, no waves are observed and we unsuccessfully tried to trigger wave trains with mechanical perturbations (but not with thermal perturbations which should be more efficient [13]).

A mechanism describing the appearance of a global mode is due to Cross [8,9] who considered the constructive effect of reflections at the boundaries. This model describes very carefully the onset of oscillatory instability in low-Prandtl-number fluids [6]. For finite reflection coefficient r, a global mode is predicted above $\epsilon_r = -s\tau_0 L^{-1} \ln|r|$. If r is zero or very small, another mechanism [3,10], but for a single wave, is to be considered: the global mode will first appear as the wave becomes absolutely unstable, i.e., above $\epsilon_{\mathrm{abs}} = \frac{1}{1+c_1^2}(\frac{s\tau_0}{2\xi_0})^2$. We need to compare ϵ_a with ϵ_r and ϵ_{abs}.

Whereas Croquette and Williams observed the first mechanism with $\epsilon_r = 0.06 < \epsilon_{\mathrm{abs}} = 0.39$ we believe our system to exhibit the second mechanism, i.e., $\epsilon_a = \epsilon_{\mathrm{abs}} < \epsilon_r$. This opinion is supported by the following set of qualitative and quantitative observations. The first argument for a low-reflection coefficient $|r|$ is the vanishing of the amplitude at $X = 0$ and $X = L$. A tentative direct measurement confirms $|r|$ to be smaller than 0.1. Quantitatively, our hypothesis $\epsilon_a = \epsilon_{\mathrm{abs}} < \epsilon_r$ leads to $|r|$ being smaller than a value located between 0.001 and 0.1, depending on τ_0's value.

The experimental sequence of competition between right and left wave with ϵ (Fig. 2) is symmetric state → asymmetric state → quasiperiodic blinking state → "filling" state, i.e., a single wave. This sequence fits the description in the case of a reflection-controlled mechanism [8,9] except that the initial symmetrical pattern exists only for $\epsilon = \epsilon_a$ and not over a finite range as in [6,9].

Let us now discuss the spatial envelope of the dominant wave. For Cross, the spatial growth rate of the global mode is $\xi_r = s\tau_0/\epsilon$, diverging at $\epsilon = 0$, not above. Wall modes are neither predicted nor observed numerically. However, for the absolute-instability mechanism, a wave shape is reported, which looks very similar to our experimental data (see Figs. 2–4 of Ref. [10]): a localized wall mode at

onset on which an invading front superimposes at higher ϵ. The main difference between our experimental data and these predictions is the simultaneous appearance—within the experimental error bar—of the front and the wall mode at ϵ_a, both structures being superimposed at any ϵ. The global mode eigenfunction [3,10] is

$$f(X) = e^{(1-ic_1)\xi_{\text{abs}}^{-1}X} \sin\pi \frac{X}{L}$$

$$\text{where } \xi_{\text{abs}} = (1 + c_1^2)\frac{2\xi_0^2}{s\tau_0}.$$

Quantitative comparison leads to a coherent description: assuming the experimental wall mode is the global mode eigenfunction $f(X)$, we identify ϵ_a with the absolute threshold ϵ_{abs}, ξ_{WM} with ξ_{abs}, and compare wave numbers at onset. Then, using the known CGL coefficients we fit $\tau_0 = (5 \pm 1)$ s and $c_1 = 0 \pm 0.5$. This value of τ_0 is very close to the viscous time $h^2/\nu = 4.5$ s. Note that, instead of linear attenuation at the downstream boundary due to the sinus in the eigenmode expression, we see an exponential decay, maybe due to nonlinear interaction between counterpropagating waves. Nevertheless, the damping in such a sink is expected to be of order of $s\tau_0\xi_0^{-2} = 0.17\ \text{mm}^{-1} = 31L^{-1}$ [8], in reasonable agreement with the measured $\xi_B^{-1} = (39 \pm 4)L^{-1}$.

Owing to the above results, we conclude that the global mode results from absolute instability transitions rather than from wave reflections.

Let us now discuss the front's critical behavior. The spatial growth scale behaves approximately as $(\epsilon - \epsilon_a)^{-1}$ (Fig. 4b, linear fit). But, the first points of Fig. 4b show a finite jump at the transition: from $1/\xi_F = 0$ at $\epsilon = 0.177$ to $(1.3 \pm 0.1)L^{-1}$ at $\epsilon = 0.181$. This quantifies the fact that the front is always present in the cell. So, we want to test other scaling laws. Following Chomaz and Couairon [16], who studied the linear or nonlinear nature of the convective/absolute transition, we checked for $(\epsilon - \epsilon_a)^{-1/2}$ (linear transition) and $\ln(\epsilon - \epsilon_a)$ (nonlinear transition) dependency for ξ_F. The $(\epsilon - \epsilon_a)^{-1/2}$ formula may be considered to fit the data very near the threshold, but the validity domain is very narrow and the fit's confidence level is very low. The logarithmic behavior is shown in Fig. 5. It appears to describe particularly well the threshold region and above up to the "saturation" region where ξ_F is limited by zero. This fit is the best of the three tested and we may conclude to a nonlinear convective/absolute transition with

$$\xi_F/L = \alpha - \beta \ln(\epsilon - \epsilon_a).$$

So, the coexistence of front mode and wall mode may be understood easily owing to the different critical behavior, square root for the wall mode vs logarithm for the front mode, the latter dominating at lowest ϵ. A similar critical behavior at the convective/absolute transition has been recently reported in an open flow: a Kelvin-Helmholtz unstable sheared interface [11].

We have presented the first complete observation of the global mode at absolute instability threshold for traveling waves in a finite closed channel. Qualitative and quantitative comparisons have been performed to distinguish this from the case of a reflection-controlled global mode. The characterization of the critical behaviors has revealed that this transition is fully nonlinear in the sense of Chomaz and Couairon [16]. For higher control parameter values, we observe a quasi-one-directional traveling pattern. This new wave train undergoes Eckhaus secondary instability leading to traveling modulations. These modulated patterns behave as nonlinear fronts whose dynamics reveals convective and absolute regimes as well [20].

We wish to thank A. Casner for his participation to the data collection; J. Burguete, F. Daviaud, J. M. Chomaz, and P. Manneville for enthusiastic discussions; and C. Gasquet for technical assistance.

*Email address: arnaud.chiffaudel@cea.fr

[1] D. Bensimon, P. Kolodner, C. Surko, H. Williams, and V. Croquette, J. Fluid Mech. **217**, 441 (1990).
[2] P. Bot, O. Cadot, and I. Mutabazi, Phys. Rev. E **58**, 3089 (1998).
[3] R. J. Deissler, J. Stat. Phys. **40**, 371 (1985).
[4] A. Couairon and J. M. Chomaz, Physica (Amsterdam) **132D**, 428 (1999).
[5] M. van Hecke, C. Storm, and W. van Saarloos, Physica (Amsterdam) **134D**, 1 (1999), and references therein.
[6] V. Croquette and H. Williams, Physica (Amsterdam) **37D**, 300 (1989).
[7] A. Chiffaudel, B. Perrin, and S. Fauve, Phys. Rev. A **39**, 2761 (1989).
[8] M. C. Cross, Phys. Rev. A **38**, 3593 (1988).
[9] M. C. Cross and E. Y. Kuo, Physica (Amsterdam) **59D**, 90 (1992).
[10] S. M. Tobias, M. R. E. Proctor, and E. Knobloch, Physica (Amsterdam) **113D**, 43 (1998).
[11] P. Gondret *et al.,* Phys. Rev. Lett. **82**, 1442 (1999).
[12] F. Daviaud and J. M. Vince, Phys. Rev. E **48**, 4432 (1993).
[13] J. M. Vince and M. Dubois, Physica (Amsterdam) **102D**, 93 (1997).
[14] N. Mukolobwiez, A. Chiffaudel, and F. Daviaud, Phys. Rev. Lett. **80**, 4661 (1998).
[15] N. Garnier, Ph.D. thesis, University Paris 7 Denis Diderot, 2000.
[16] J. M. Chomaz and A. Couairon, Phys. Fluids **11**, 2977 (1999).
[17] N. Garnier, A. Chiffaudel, A. Prigent, and F. Daviaud (to be published). The onset value 3.5 K announced in [14] was overestimated due to few data collected on the sideband. The actual value refers to more than 100 data points.
[18] M. K. Smith, J. Fluid Mech. **194**, 391 (1988).
[19] M. A. Pelacho, A. Garcimartin, and J. Burguete, Phys. Rev. E **62**, 477 (2000).
[20] N. Garnier, A. Chiffaudel, and F. Daviaud (to be published).